Nonlinear Vehicle Side-Slip Estimation with Friction Adaptation ⋆

Håvard Fjær Grip [a,c] Lars Imsland [a] Tor A. Johansen [a,c] Thor I. Fossen [a,c]
Jens C. Kalkkuhl [b] Avshalom Suissa [b]

[a] *SINTEF ICT, Applied Cybernetics, NO-7465 Trondheim, Norway*

[b] *DaimlerChrysler AG, 71059 Sindelfingen, Germany*

[c] *NTNU, Department of Engineering Cybernetics, NO-7491 Trondheim, Norway*

Abstract

A nonlinear observer for estimation of the longitudinal velocity, lateral velocity, and yaw rate of a vehicle, designed for the purpose of vehicle side-slip estimation, is modified and extended in order to work for different road surface conditions. The observer relies on a road-tire friction model and is therefore sensitive to changes in the adhesion characteristics of the road surface. The friction model is parametrized with a single friction parameter, and an update law is designed. The adaptive observer is proven to be uniformly globally asymptotically stable and uniformly locally exponentially stable under a persistency-of-excitation condition and a set of technical assumptions, using results related to Matrosov's theorem. The observer is tested on recorded data from two test vehicles and shows good results on a range of road surfaces.

Key words: side-slip estimation, automotive vehicles, nonlinear observers, velocity estimation, friction

1 Introduction

A current focus of the automotive industry is the development of active safety systems, which assist the driver in order to avoid dangerous situations. As such systems become more advanced, they depend to an increasing extent on accurate information about the state of the vehicle and its surroundings. Much of this information can be obtained by direct measurement, but the appropriate sensors may be unreliable, inaccurate, or prohibitively expensive. Observers are therefore used to provide accurate and reliable estimates of important states.

Observers that estimate vehicle velocity usually rely on road-tire friction models, which model the friction forces between the tires of the vehicle and the road surface. As the adhesion characteristics between the tires and the road depend on the road surface, knowledge about the current road surface conditions is important for this type of observer to work properly.

Several different methods for obtaining information about road surface conditions have previously been studied. In Ono, Asano, Sugai, Ito, Yamamoto, Sawada, and Yasui (2003), a least-squares method is used on measurements of wheel angular velocity to estimate the slope of the friction force versus the tire slip. An observer for lateral velocity in Fukada (1999) includes a filtering scheme for estimating the maximum road-tire friction coefficient, based primarily on using the lateral acceleration measurement during times when this provides a good measurement of the coefficient. A similar approach is taken in Hac and Simpson (2000). In Gustafsson (1997), a Kalman filter is used to classify road surface conditions, by inspecting the ratio between slip values of the driven wheels and the normalized friction force, obtained using wheel angular velocities and engine torque. In Ray (1997), an extended Kalman filter (EKF) is combined with statistical methods in order to estimate the maximum road-tire friction coefficient, using measurements of the yaw and roll rates, wheel angular velocities, and longitudinal and lateral accelerations, as well as knowledge of the steering angle and total brake line pressure. Other examples of EKFs are presented in Suissa, Zomotor, and Böttiger (1994) and Best, Gordon, and Dixon (2000). In Nishira, Kawabe, and Shin (1999), wheel angular velocity, longitudinal tire slip, and wheel torque is used to generate an estimate of the wheel angular velocity and for adaptation of a friction parameter. Wheel angular velocity and torque is used in Canudas-de-Wit, Petersen, and Shiriaev (2003) for estimation of the longitudinal velocity and wheel

⋆ This research is supported by the European Commission STREP project CEmACS, contract 004175.

Email address: grip@itk.ntnu.no (Håvard Fjær Grip).

angular velocity, and adaptation of a friction parameter. In both Nishira et al. (1999) and Canudas-de-Wit et al. (2003), convergence of the adapted friction parameters under conditions of nonzero longitudinal tire slip is studied.

In addition to accuracy and reliability, production cost is an important matter in vehicle serial production. To reduce cost, observer designs should be computationally efficient and be based on cheap sensor configurations. In Imsland, Johansen, Fossen, Grip, Kalkkuhl, and Suissa (2006a), a nonlinear observer for vehicle velocity is presented with stability guarantees. The observer is computationally efficient and is based on measurements commonly available in modern cars. A significant weakness of the observer is that it relies on a friction model that must be tuned to the current road surface conditions. In Grip, Imsland, Johansen, Fossen, Kalkkuhl, and Suissa (2006), the authors addressed this issue for a reduced-order observer for lateral velocity by presenting a method for adaptation of the friction model to different road surface conditions. In the current paper, an improved version of this adaptive observer is presented, and in Section 5, it is extended to include longitudinal velocity and yaw rate. The observer retains the advantage of being less computationally expensive than an EKF. The ultimate goal of the observer design is accurate estimation of the vehicle side-slip angle.

The stability analysis presented in this paper relies crucially on the concept of persistency of excitation (PE), introduced by Åström and Bohlin (1965). This concept has been developed in various directions to deal with situations where regressors are dependent not only on external, time-varying signals, but on the states of the system, which is the case for the system considered in this paper. One approach to dealing with state-dependent regressors is to consider a PE condition along the trajectories of the states. The drawback of this approach is that, in general, the trajectories of the states must be known in advance. Another approach is to consider the states a parameter, and to evaluate a PE condition over all values of this parameter. This idea is combined with a generalization of Matrosov's theorem in Loría, Panteley, Popović, and Teel (2005), the results of which are used in this paper. Although the specific trajectories of the states need not be known, the PE conditions resulting from this approach are in general difficult to verify. In the present case, we nevertheless offer a natural and intuitively reasonable interpretation of the PE condition, which is directly related to driving patterns and supported by experimental results.

Systems similar to the one considered in this paper have previously been investigated under PE conditions (Ortega and Fradkov, 1993; Zhang, Ioannou, and Chien, 1996; Panteley, Loría, and Teel, 2001). Another example of observer design with analysis similar to what is presented here can be found in Loría and de León Morales (2003).

1.1 Notation

Conventional notation is used for denoting estimated variables and error variables, meaning that for some variable z, $\hat{z}$ denotes its estimate and $\tilde{z} = z - \hat{z}$. When considering error dynamics, a function depending on an estimated variable $\hat{z}$ may be written as a function of the error variable $\tilde{z}$ and t, by noting that $\hat{z} = z - \tilde{z}$ and considering z a time-varying signal. For a vector z, $z_{\{i,j\}}$ denotes the vector obtained by stacking elements i and j of z. The norm operator $\|\cdot\|$ denotes the Euclidian norm. The closed ball with center 0 and radius r is denoted $\overline{B}(r) = \{z \mid \|z\| \leq r\}$. The minimum eigenvalue of a matrix A is denoted $\lambda_{\min}(A)$. The positive real numbers are denoted $\mathbb{R}_{>0}$.

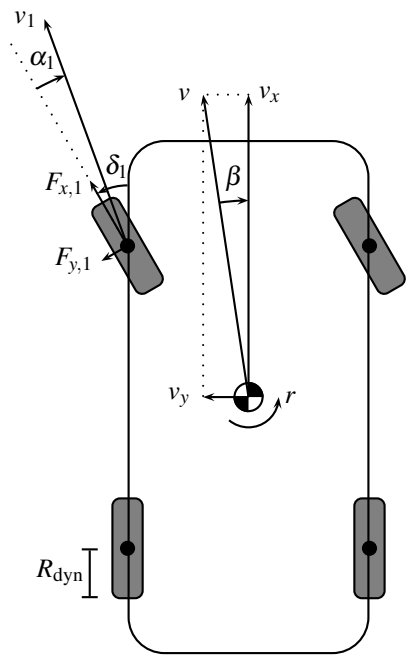

Fig. 1. Schematic overview of vehicle

2 Vehicle Model and Preliminaries

The vehicle is illustrated in Figure 1. Of primary interest is the side-slip angle β, which is the angle between the longitudinal direction of the vehicle and the direction of travel at the center of gravity (CG). To obtain the side-slip angle, we shall estimate the longitudinal velocity v_x and the lateral velocity v_y at the CG, from which $\beta = -\arctan(v_y/v_x)$ can be calculated.

The vehicle is assumed to be moving on a flat, horizontal surface. In general, there are environmental forces, such as wind forces and air resistance, acting on the vehicle. In our model, these are disregarded; we assume that only road-tire friction forces act on the vehicle.

2.1 Friction Modeling

Several semi-empirical models for road-tire friction exist, the most well-known of which is the Magic Formula (Pacejka, 2006). This paper is not based on a particular friction

model; instead, it is assumed that the friction model adheres to certain assumptions, which will be formally stated later. Thus, the design is not bound to a particular friction model, but instead allows for a range of friction models to be used.

Road-tire friction forces are usually calculated based on the normal force between a tire and the road, and tire slip values. The tire slip values are measures of the relative difference between the vehicle velocity and the circumferential velocity of the tire in its longitudinal and lateral directions. Exact definitions of tire slips vary, but one possible definition, used for the experimental results in this paper, is

$$\lambda_{x,i} = \frac{\omega_i R_{\text{dyn}} - \|v_i\| \cos\alpha_i}{\|v_i\|}, \quad \lambda_{y,i} = \sin\alpha_i,$$

where $\lambda_{x,i}$ and $\lambda_{y,i}$ are the longitudinal and lateral slips of wheel number i; R_{dyn} is the dynamic radius of the tire; ω_i is the angular velocity of the wheel; v_i is the velocity vector of the vehicle above the wheel center; and α_i is the angle between the longitudinal direction of the wheel and the vector v_i (see illustration of front-left wheel in Figure 1).

It is common to define the friction coefficient $\mu = F/F_z$, where F is the magnitude of the road-tire friction force and F_z is the magnitude of the vertical normal force. Everything else being the same, μ is in general lower on more slippery surfaces. The value μ is, however, not constant for a particular surface. The road surface conditions are therefore more suitably described by the maximum value of μ for a particular surface. Throughout this paper, μ_H is used to denote some parameter used in the friction model to characterize the road-tire friction properties, usually the maximum road-tire friction coefficient.

In the following, we denote by d a vector containing all time-varying signals used in the friction model, except the lateral velocity v_y and the coefficient μ_H. The contents of d may be different depending on the friction model used, but we assume availability of certain measurements to be included in d:

- the longitudinal acceleration (a_x)
- the lateral acceleration (a_y)
- the yaw rate (r)
- the wheel angular velocities (ω_i, $i = 1,\ldots,4$)
- the wheel angles (δ_i, $i = 1,\ldots,4$)

The wheel angles δ_i are in practice calculated from the measured steering wheel angle δ. Because estimation of the longitudinal velocity v_x is not considered until Section 5, it is at this point assumed available as a measurement and included in d. We denote the friction forces by vector-valued functions $F_i(d, v_y, \mu_H)$.

2.2 Vehicle Model

The vehicle is modeled as a rigid body and is studied in a body-fixed coordinate system with the origin located at the CG. The friction forces $F_i(d, v_y, \mu_H)$ are calculated in wheel-fixed coordinate systems, rotated by angles δ_i with respect to the body-fixed one. The resultant force acting on the vehicle in the lateral direction is denoted

$$f_y(d, v_y, \mu_H) = \sum_{i=1}^{4} [0\ 1] R(\delta_i) F_i(d, v_y, \mu_H),$$

where $R(\delta_i)$ are rotational matrices between the wheel-fixed coordinate systems and the body-fixed one. Using Newton's second law, we may write $ma_y = f_y(d, v_y, \mu_H)$, where m is the mass of the vehicle. The equation of motion in the lateral direction is (see, e.g., Kiencke and Nielsen, 2000)

$$\dot{v}_y = a_y - r v_x. \tag{1}$$

3 Adaptive Observer

In Imsland et al. (2006a), the lateral velocity part of the observer includes a stabilizing injection term that relies on the friction model. The friction model is assumed to be tuned to the current road surface conditions. This assumption is now removed, and a method is developed for adaptation of the friction model to different road surface conditions.

3.1 Friction Model Parametrization

It is necessary to identify one or more parameters that characterize different road surface conditions and tire properties, and which are suitable for adaptation. One possibility is to use μ_H for adaptation, as is done in Grip et al. (2006). In this paper, a closely related parameter, which is easier to deal with and results in slightly better performance, is chosen. We may write

$$f_y(d, v_y, \mu_H) = \theta f_y^*(d, v_y), \tag{2}$$

where θ is the parameter to be adapted. The function f_y^* is defined as

$$f_y^*(d, v_y) = \frac{1}{\mu_H^*} \sum_{i=1}^{4} [0\ 1] R(\delta_i) F_i(d, v_y, \mu_H^*),$$

where μ_H^* is some fixed nominal value of μ_H.

Assumption 1 *The friction parameter θ is constant and strictly positive, with known upper and lower bounds, such that $\dot{\theta} = 0$ and $0 < \theta_{\min} \leq \theta \leq \theta_{\max}$.*

Compared to using μ_H for adaptation, choosing θ as described above offers certain benefits, because the parameter enters linearly into (2). The drawback of the chosen parametrization is that Assumption 1 is less realistic, since θ cannot be expected to be completely time-invariant even if the road surface conditions remain unchanged. In order to compare the two parameters μ_H and θ, Figure 2 shows the magnitude of the calculated friction force in the lateral

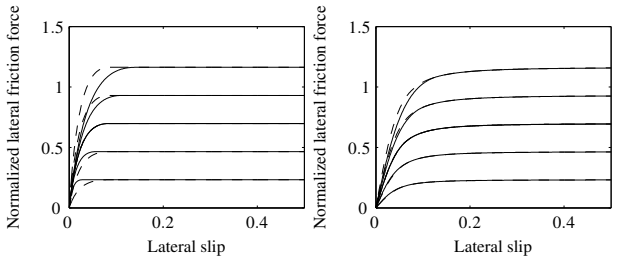

(a) Zero longitudinal tire slip (b) Longitudinal slip set to 0.05

Fig. 2. Friction curves for different friction parameters (dashed) and μ_H (solid)

direction of a single wheel, normalized by division with the normal force F_z. The solid curves are generated using different values of μ_H in the friction model, while the dashed curves are generated by using a nominal coefficient $\mu_H^* = 0.6$ and varying θ. [1]

The difference seen in Figure 2 may result in rapid variations in the friction parameter when the driving pattern is highly varied. This is illustrated in Figure 3, where θ is plotted for simulated maneuvers with increasingly rapid variations on a high-friction ($\mu_H = 1.0$) and a low-friction ($\mu_H = 0.3$) surface. Assumption 1 must be seen as a necessary design assumption, which is known to be an imprecise description of the true physical system. While a varied driving pattern causes variation in θ, it also results in greater robustness of the observer to be presented, as will be shown in Section 4. Moreover, experimental results indicate that the observer is indeed robust with respect to the error made in making this assumption.

Using a single parameter to describe different road surfaces is a simplification of the true physical system. Such a parametrization cannot, for example, describe situations where the surface is different below each wheel. For the lateral velocity estimation in this paper it is, however, enough to identify the effect of surface changes on the resultant lateral force, without regard to how this manifests itself physically (this is no longer true when yaw rate estimation is added, but given that feedback from the yaw rate measurement is available, this does not present significant problems). While a design could be based on a richer parametrization, for example by using one parameter per wheel, separate ones for the lateral resultant force and yaw moment, or by expressing the friction model in terms of several basis functions, the added complexity does not seem warranted in light of the good results obtained using the simple one-parameter scheme.

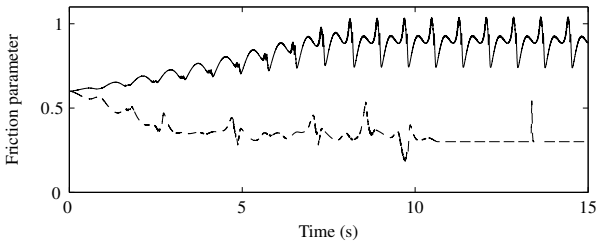

Fig. 3. Friction parameter for maneuver on high-friction (solid) and low-friction (dashed) surface

3.2 Observer and Stability Results

Before proposing an observer and presenting stability results, some extra assumptions are needed. We define the vector $x = [v_y, \theta]^\mathsf{T}$ of states to be estimated.

Assumption 2 *There exist compact sets $D_d \subset \mathbb{R}^m$ and $D_{v_y} \subset \mathbb{R}$ such that*

- $(d, v_y) \in D_d \times D_{v_y}$;
- *d and v_y are uniformly continuous in t on $\mathbb{R}$; and*
- *$F_i(d, v_y, \mu_H^*)$ and $[\partial F_i/\partial v_y](d, v_y, \mu_H^*)$ are continuous on $D_d \times \mathbb{R} \times \{\mu_H^*\}$.*

Assumption 3 *There exists a known function $\xi : D_d \times \mathbb{R}^2 \to \mathbb{R}$ such that $\xi(d,\hat{x})$ and $[\partial\xi/\partial\hat{x}](d,\hat{x})$ are continuous on $D_d \times \mathbb{R}^2$ and*

$$f_y^*(d, v_y) - f_y^*(d, \hat{v}_y) = \xi(d,\hat{x})(v_y - \hat{v}_y). \tag{3}$$

Remark 1 According to the mean value theorem, there always exists a value such that (3) holds if $\xi(d,\hat{x})$ is given that value. In general it is, however, not possible to obtain this exact value without knowing v_y. Fortunately, it is not difficult to obtain a sufficiently good approximation of the value, as will be discussed in Section 6. □

For presentation of the error dynamics, we define the function

$$\tilde{a}_y(t,\tilde{x}) = a_y - \frac{1}{m}\hat{\theta} f_y^*(d, \hat{v}_y).$$

This represents the difference between the actual lateral acceleration and an estimate obtained using the friction model. The notation $\hat{f}_y^* = f_y^*(d, \hat{v}_y)$, $\xi = \xi(d,\hat{x})$, and $\tilde{a}_y = \tilde{a}_y(t,\tilde{x})$ is used for the sake of brevity.

The following observer is proposed:

$$\dot{\hat{v}}_y = a_y - r v_x + K_{v_y}\Lambda\xi\left(m a_y - \hat{\theta}\hat{f}_y^*\right), \tag{4a}$$

$$\dot{\hat{\theta}} = \Gamma K_{v_y}\Lambda\hat{f}_y^*\left(m a_y - \hat{\theta}\hat{f}_y^*\right), \tag{4b}$$

[1] The comparison in Figure 2 is for a single wheel. In most practical situations, the friction forces for each wheel are different, and some of the difference in parametrization will average out in the resultant force.

where K_{v_y} and Γ are positive gains and $\Lambda = \Lambda(d,\hat{x})$ refers to some choice function $\Lambda\colon D_d \times \mathbb{R}^2 \to [\Lambda_{\min}, \Lambda_{\max}] \subset \mathbb{R}_{>0}$, defined such that $\Lambda(d,\hat{x})$ and $[\partial\Lambda/\partial\hat{x}](d,\hat{x})$ are continuous on $D_d \times \mathbb{R}^2$. This function is used to scale the observer equations for numerical reasons, and its exact shape is not important for the stability analysis. Subtracting (4a) from (1) we obtain the following error dynamics:

$$\dot{\tilde{v}}_y = -K_{v_y} m \Lambda \xi \tilde{a}_y, \tag{5a}$$

$$\dot{\tilde{\theta}} = -\Gamma K_{v_y} m \Lambda \hat{f}_y^* \tilde{a}_y. \tag{5b}$$

Assumptions 1–3 imply that the right-hand side of (5) is continuous in t and locally Lipschitz continuous in $\tilde{x}$, uniformly in t.

Lemma 1 *If Assumptions 1–3 hold, then the origin of the error dynamics* (5) *is uniformly globally stable* (UGS). □

PROOF We define a Lyapunov function candidate (LFC)

$$V(\tilde{x}) = \frac{1}{2m^2}\left(\theta\Gamma\tilde{v}_y^2 + \tilde{\theta}^2\right),$$

which is positive definite and radially unbounded. Its time derivative along the trajectories of (5) is

$$\dot{V}(t,\tilde{x}) = -\frac{1}{m}\Gamma K_{v_y}\Lambda\tilde{a}_y\left(\theta\xi\tilde{v}_y + \hat{f}_y^*\tilde{\theta}\right).$$

We may write

$$m\tilde{a}_y = \theta\left(f_y^*(d,v_y) - \hat{f}_y^*\right) + \hat{f}_y^*\tilde{\theta} = \theta\xi\tilde{v}_y + \hat{f}_y^*\tilde{\theta}.$$

Using this for substitution yields

$$\dot{V}(t,\tilde{x}) = -\Gamma K_{v_y}\Lambda\tilde{a}_y^2 \le -\Gamma K_{v_y}\Lambda_{\min}\tilde{a}_y^2.$$

It follows that the origin of (5) is UGS (see, e.g., Loría et al., 2005, Def. 1). ■

Building on Lemma 1, uniform global asymptotic stability (UGAS) of the origin of the error dynamics (5) is proven in the following theorem, subject to an excitation condition that will be extensively discussed. We define the functions

$$\eta_{v_y}(t,\tilde{v}_y) = \begin{cases} \frac{1}{m}\theta\frac{f_y^*(d,v_y) - f_y^*(d,\hat{v}_y)}{\tilde{v}_y}, & \tilde{v}_y \neq 0; \\ \frac{1}{m}\theta\frac{\partial f_y^*}{\partial v_y}(d,v_y), & \tilde{v}_y = 0, \end{cases} \tag{6}$$

$$\eta_\theta(t,\tilde{v}_y) = \frac{1}{m}f_y^*(d,\hat{v}_y). \tag{7}$$

Using these functions, we may write

$$\tilde{a}_y = \eta_{v_y}(t,\tilde{v}_y)\tilde{v}_y + \eta_\theta(t,\tilde{v}_y)\tilde{\theta}. \tag{8}$$

Hence, $\eta_{v_y}(t,\tilde{v}_y)$ and $\eta_\theta(t,\tilde{v}_y)$ are measures of the influence of $\tilde{v}_y$ and $\tilde{\theta}$ on $\tilde{a}_y$.

Theorem 1 (UGAS of lateral velocity observer) *Suppose that for each $\tilde{v}_y \in \mathbb{R}$, there exist $T > 0$ and $\varepsilon > 0$ such that for all $t \in \mathbb{R}$,*

$$\int_t^{t+T}\eta_{v_y}^2(\tau,\tilde{v}_y)\,\mathrm{d}\tau\int_t^{t+T}\eta_\theta^2(\tau,\tilde{v}_y)\,\mathrm{d}\tau - \left(\int_t^{t+T}\eta_{v_y}(\tau,\tilde{v}_y)\eta_\theta(\tau,\tilde{v}_y)\,\mathrm{d}\tau\right)^2 > \varepsilon. \tag{9}$$

If Assumptions 1–3 hold, then the origin of the error dynamics (5) *is* UGAS. □

Remark 2 The condition expressed by (9) concerns the relationship between the two signals $\eta_{v_y}(\cdot,\tilde{v}_y)$ and $\eta_\theta(\cdot,\tilde{v}_y)$. To see this, it is useful to note that according to the Cauchy-Schwartz inequality, the left-hand side is always non-negative, and it is positive if and only if the continuous signals $\eta_{v_y}(\cdot,\tilde{v}_y)$ and $\eta_\theta(\cdot,\tilde{v}_y)$ are linearly independent on $[t,t+T]$ (see, e.g., Young, 1988, Theorem 1.9). Loosely speaking, the condition can be fulfilled by guaranteeing that the signals vary in a sufficiently independent manner within such time windows. In practical terms, this amounts to requiring that the driving pattern is somewhat varied, not consisting of indefinitely long periods of driving along a straight path or in a circle at constant speed.[2] This is discussed in detail in Section 7. □

PROOF (THEOREM 1) From Lemma 1, we know that the origin of the error dynamics is UGS. We may therefore use Loría et al. (2005, Theorem 4). The function $\tilde{a}_y$ is locally Lipschitz continuous in $\tilde{x}$, uniformly in t. Hence, for each $\Delta > 0$, there exists a $\mu > 0$ such that for all $(t,\tilde{x}) \in \mathbb{R}\times\overline{B}(\Delta)$, $\max\left\{|V(\tilde{x})|, |\tilde{a}_y|\right\} \le \mu$, where V is the Lyapunov function from the proof of Lemma 1. We define $Y\colon \mathbb{R}^2\times\mathbb{R}\to\mathbb{R}$ as

$$Y(z,\psi) = -\Gamma K_{v_y}\Lambda_{\min}\psi^2.$$

We have that $\dot{V}(t,\tilde{x}) \le Y(\tilde{x},\tilde{a}_y)$, $Y(z,\psi) \le 0$, and $Y(z,\psi) = 0 \implies \psi = 0$.

We may write

$$\int_t^{t+T}\tilde{a}_y^2(\tau,\tilde{x})\,\mathrm{d}\tau = \tilde{x}^{\mathrm{T}}W(t,\tilde{v}_y)\tilde{x},$$

where

$$W(t,\tilde{v}_y) = \int_t^{t+T}\begin{bmatrix}\eta_{v_y}^2(\tau,\tilde{v}_y) & \eta_{v_y}(\tau,\tilde{v}_y)\eta_\theta(\tau,\tilde{v}_y)\\ \eta_{v_y}(\tau,\tilde{v}_y)\eta_\theta(\tau,\tilde{v}_y) & \eta_\theta^2(\tau,\tilde{v}_y)\end{bmatrix}\mathrm{d}\tau.$$

Note that for each $\tilde{v}_y$, $\eta_{v_y}(\tau,\tilde{v}_y)$ and $\eta_\theta(\tau,\tilde{v}_y)$ are uniformly bounded. The second-order leading principal minor (or de-

[2] It is important to note (i) that $\tilde{v}_y = 0$ does not imply that either signal is zero, and (ii) that the condition may hold even if one or both of the signals are zero for limited periods of time.

terminant) of $W(t,\tilde{v}_y)$ is

$$\int_t^{t+T} \eta_{v_y}^2(\tau,\tilde{v}_y)\,\mathrm{d}\tau \int_t^{t+T} \eta_\theta^2(\tau,\tilde{v}_y)\,\mathrm{d}\tau - \left(\int_t^{t+T} \eta_{v_y}(\tau,\tilde{v}_y)\eta_\theta(\tau,\tilde{v}_y)\,\mathrm{d}\tau\right)^2.$$

From (9), this expression evaluates to some value greater than ε. The first-order leading principal minor of $W(t,\tilde{v}_y)$ is $\int_t^{t+T} \eta_{v_y}^2(\tau,\tilde{v}_y)\,\mathrm{d}\tau$, which is obviously non-negative. It is also nonzero because the determinant would otherwise be zero. Hence, for each $\tilde{v}_y$, $W(t,\tilde{v}_y)$ is positive definite with a uniformly lower bounded determinant and upper bounded eigenvalues, which means that $\lambda_{\min}(W(t,\tilde{v}_y)) > \varepsilon' > 0$ for some ε'. Therefore, for all $t \in \mathbb{R}$, $\int_t^{t+T} \tilde{a}_y^2(\tau,\tilde{x})\,\mathrm{d}\tau \geq \varepsilon'\|\tilde{x}\|^2$. Boundedness of the integrand for each $\tilde{x}$ in turn implies that for each $\tilde{x} \neq 0$, there exist $\varepsilon^* > 0$ and $T > 0$ such that for all $t \in \mathbb{R}$, $\int_t^{t+T} |\tilde{a}_y(\tau,\tilde{x})|\,\mathrm{d}\tau \geq \varepsilon^*$. This means that $\tilde{a}_y$ is uniformly δ-persistently exciting (Uδ-PE) with respect to $\tilde{x}$ by Loría et al. (2005, Lemma 1), and it is also zero for $\tilde{x} = 0$.

The right-hand sides of (5a) and (5b) consist of $\tilde{a}_y$ multiplied by factors that are bounded for all $(t,\tilde{x}) \in \mathbb{R} \times \overline{B}(\Delta)$. Hence, there exists a constant $K_1(\Delta)$ such that for all $(t,\tilde{x}) \in \mathbb{R} \times \overline{B}(\Delta)$, $\|g(t,\tilde{x})\| \leq K_1(\Delta)|\tilde{a}_y|$, where $g(t,\tilde{x})$ denotes the right-hand side of (5). ∎

The observer (4) allows the estimated friction parameter $\hat{\theta}$ to take on any value, but from physical considerations, we know that θ is confined to a small region, as reflected by Assumption 1. We may use this extra knowledge by implementing a parameter projection (see, e.g., Ioannou and Sun, 1996), while preserving the stability properties of the error dynamics. Doing so, we may ensure that for all $t \geq t_0$, $\theta_{\min} - \theta_\varepsilon \leq \hat{\theta} \leq \theta_{\max} + \theta_\varepsilon$ (where $\theta_\varepsilon > 0$ is some arbitrarily small constant), as long as $\hat{\theta}$ is within those bounds at $t = t_0$ (see Grip et al., 2006).

4 Robustness

Equilibrium points with the UGAS property are locally input-to-state stable and therefore robust to small perturbations, as mentioned in Loría et al. (2005). By using a different LFC, which includes a term similar to one of the auxiliary functions used in the proof of Loría et al. (2005, Theorem 4), we obtain a stronger local stability result. The approach is similar to the proof of Loría, Panteley, Popović, and Teel (2006, Propositions 3 and 4), where uniform local exponential stability (ULES) is proven for a particular class of systems.

Theorem 2 (ULES of lateral velocity observer) *Suppose that Assumptions 1–3 and the condition expressed by* (9) *hold. Then the origin of the error dynamics* (5) *is* ULES. □

PROOF We define the LFC

$$V_{\mathrm{PE}}(t,\tilde{x}) = V(\tilde{x}) - \gamma \int_t^\infty \mathrm{e}^{t-\tau}\,\tilde{a}_y^2(\tau,\tilde{x})\,\mathrm{d}\tau,$$

where $\gamma > 0$ is a constant and V is the Lyapunov function from the proof of Lemma 1. In the remainder of the proof, it is assumed that $\tilde{x} \in \overline{B}(\Delta)$ for some arbitrary $\Delta > 0$. Because $\tilde{a}_y$ is locally Lipschitz continuous in $\tilde{x}$, uniformly in t, and zero for $\tilde{x} = 0$, there exists a $K_2(\Delta)$ such that $|\tilde{a}_y| \leq K_2(\Delta)\|\tilde{x}\|$. We therefore have

$$\begin{aligned} V_{\mathrm{PE}}(t,\tilde{x}) &\geq \frac{1}{2m^2}\left(\theta\Gamma\tilde{v}_y^2 + \tilde{\theta}^2\right) - \gamma K_2^2(\Delta)\|\tilde{x}\|^2 \int_t^\infty \mathrm{e}^{t-\tau}\,\mathrm{d}\tau \\ &\geq \left(\frac{1}{2m^2}\min\{1,\theta\Gamma\} - \gamma K_2^2(\Delta)\right)\|\tilde{x}\|^2. \end{aligned}$$

Choosing $\gamma < \min\{1,\theta\Gamma\}/(2m^2K_2^2(\Delta))$ ensures that V_{PE} is positive definite and bounded:

$$\left(\frac{1}{2m^2}\min\{1,\theta\Gamma\} - \gamma K_2^2(\Delta)\right)\|\tilde{x}\|^2 \leq V_{\mathrm{PE}}(t,\tilde{x}) \leq \frac{1}{2m^2}\max\{1,\theta\Gamma\}\|\tilde{x}\|^2. \quad (10)$$

For the time derivative along the trajectories of (5), we have

$$\begin{aligned} \dot{V}_{\mathrm{PE}}(t,\tilde{x}) \leq &-\left(\Gamma K_{v_y}\Lambda_{\min} - \gamma\right)\tilde{a}_y^2 - \gamma\int_t^\infty \mathrm{e}^{t-\tau}\,\tilde{a}_y^2(\tau,\tilde{x})\,\mathrm{d}\tau \\ &- 2\gamma\int_t^\infty \mathrm{e}^{t-\tau}\,\tilde{a}_y(\tau,\tilde{x})\frac{\partial\tilde{a}_y}{\partial\tilde{x}}(\tau,\tilde{x})\,\mathrm{d}\tau\, g(t,\tilde{x}), \end{aligned}$$

where $g(t,\tilde{x})$ denotes the right-hand side of (5). The continuity properties of the friction model imply that $\|[\partial\tilde{a}_y/\partial\tilde{x}](t,\tilde{x})\| \leq K_3(\Delta)$. It can be shown that the left-hand side of (9) is continuous in $\tilde{v}_y$, uniformly in t, which means that $[-\Delta,\Delta]$ is covered by open neighborhoods around each $\tilde{v}_y$ for which (9) holds with the same T and ε. Since $[-\Delta,\Delta]$ is compact, this cover has finite subcover, and hence we may choose $T_\Delta > 0$ and $\varepsilon_\Delta > 0$ such that (9) holds uniformly for all $(t,\tilde{x}) \in \mathbb{R} \times \overline{B}(\Delta)$ with $T = T_\Delta$ and $\varepsilon = \varepsilon_\Delta$. Defining W as in the proof of Theorem 1 with $T = T_\Delta$ and using the boundedness property of the elements of $W(t,\tilde{v}_y)$ on $\mathbb{R} \times \overline{B}(\Delta)$, we may define ε'_Δ accordingly, such that

$$\int_t^{t+T_\Delta} \tilde{a}_y^2(\tau,\tilde{x})\,\mathrm{d}\tau = \tilde{x}^{\mathrm{T}}W(t,\tilde{v}_y)\tilde{x} \geq \varepsilon'_\Delta\|\tilde{x}\|^2.$$

From this, we may write

$$\begin{aligned} \dot{V}_{\mathrm{PE}}(t,\tilde{x}) \leq &-\left(\Gamma K_{v_y}\Lambda_{\min} - \gamma\right)\tilde{a}_y^2 - \gamma\varepsilon'_\Delta\,\mathrm{e}^{-T_\Delta}\|\tilde{x}\|^2 \\ &+ 2\gamma K_1(\Delta)K_2(\Delta)K_3(\Delta)\|\tilde{x}\||\tilde{a}_y|, \end{aligned} \quad (11)$$

where $K_1(\Delta)$ is defined in the proof of Theorem 1. Selecting

$$\gamma < \frac{\Gamma K_{v_y}\Lambda_{\min}}{1 + K_1^2(\Delta)K_2^2(\Delta)K_3^2(\Delta)\varepsilon_\Delta'^{-1}\,\mathrm{e}^{T_\Delta}}$$

ensures that $\dot{V}_{\mathrm{PE}}(t,\tilde{x})$ is negative definite and bounded by

$$\dot{V}_{\mathrm{PE}}(t,\tilde{x}) \leq -c\left(\|\tilde{x}\|^2 + |\tilde{a}_y|^2\right),$$

for some $c > 0$. This can be seen by writing (11) in quadratic, symmetric matrix form and investigating the leading principal minors. According to Khalil (2002, Theorem 4.10), the origin of (5) is therefore ULES. ■

The combination of UGAS and ULES implies that the system is uniformly exponentially stable within any compact neighborhood of the origin, and hence it is unnecessary to investigate the region of attraction in Theorem 2. The proof indicates that the stability margin depends on the amount of excitation in the system.

5 Extension to Longitudinal Velocity and Yaw Rate

The adaptive observer design is now extended to include estimation of longitudinal velocity and yaw rate. The vector d is redefined to exclude the values v_x and r, and these values are instead used as explicit arguments to F_i. The vehicle model for the longitudinal velocity and yaw rate can be written as

$$\begin{aligned} \dot{v}_x &= a_x + r v_y, \\ \dot{r} &= \frac{1}{J} f_r(d, v_x, v_y, r, \mu_H), \end{aligned}$$

where J is the vehicle moment of inertia around the vertical axis through the CG. The function f_r represents the yaw moment, and we assume that it can be expressed as $f_r(d, v_x, v_y, r, \mu_H) = \theta f_r^*(d, v_x, v_y, r)$, where

$$f_r^*(d, v_x, v_y, r) = \frac{1}{\mu_H^*} \sum_{i=1}^{4} g_i^{\mathsf{T}} R(\delta_i) F_i(d, v_x, v_y, r, \mu_H^*).$$

The vectors g_i are geometry vectors defined for convenience (see Imsland et al., 2006a).

Remark 3 Using the same type of parametrization, and the same parameter, for calculation of the yaw moment as for the lateral acceleration is a significant simplification, because different tire slip values for the front and rear wheels will give the difference seen in Figure 2 much more impact. In normal driving situations without large tire slip values, one may therefore expect large inaccuracies. Essentially the same design as the one given in this paper can, however, be implemented with adaptation of μ_H instead, albeit at the cost of making other assumptions (see Imsland, Grip, Johansen, Fossen, Kalkkuhl, and Suissa, 2007). The choice of the best parametrization for a final implementation is a topic of current research. □

We now write

$$f_y^*(d, v_x, v_y, r) = \frac{1}{\mu_H^*} \sum_{i=1}^{4} [0\ 1] R(\delta_i) F_i(d, v_x, v_y, r, \mu_H^*).$$

The vector x is defined as $x = [v_x, v_y, r, \theta]^{\mathsf{T}}$ and Assumptions 2 and 3 now take the following form:

Assumption 2′ *There exist compact sets $D_d \subset \mathbb{R}^m$, $D_{v_x} \subset \mathbb{R}$, $D_{v_y} \subset \mathbb{R}$ and $D_r \subset \mathbb{R}$ such that*

- *$(d, v_x, v_y, r) \in D_d \times D_{v_x} \times D_{v_y} \times D_r$;*
- *d, v_x, v_y, and r are uniformly continuous in t on $\mathbb{R}$;*
- *$F_i(d, v_x, v_y, r, \mu_H^*)$ and their partial derivatives with respect to v_x, v_y, and r are continuous on $D_d \times \mathbb{R} \times \mathbb{R} \times \mathbb{R} \times \{\mu_H^*\}$; and*
- *$[\partial F_i/\partial v_x](d, v_x, v_y, r, \mu_H^*)$ and $[\partial F_i/\partial r](d, v_x, v_y, r, \mu_H^*)$ are uniformly bounded on $D_d \times \mathbb{R} \times D_{v_y} \times \mathbb{R} \times \{\mu_H^*\}$.*

Assumption 3′ *There exist known functions $\xi : D_d \times \mathbb{R}^4 \to \mathbb{R}$ and $\zeta : D_d \times \mathbb{R}^4 \to \mathbb{R}$ such that $\xi(d,\hat{x})$, $\zeta(d,\hat{x})$, $[\partial\xi/\partial\hat{x}](d,\hat{x})$, and $[\partial\zeta/\partial\hat{x}](d,\hat{x})$ are continuous on $D_d \times \mathbb{R}^4$ and*

$$f_y^*(d, \hat{v}_x, v_y, \hat{r}) - f_y^*(d, \hat{v}_x, \hat{v}_y, \hat{r}) = \xi(d,\hat{x})(v_y - \hat{v}_y), \quad (12)$$

$$f_r^*(d, \hat{v}_x, v_y, \hat{r}) - f_r^*(d, \hat{v}_x, \hat{v}_y, \hat{r}) = \zeta(d,\hat{x})(v_y - \hat{v}_y). \quad (13)$$

We redefine $\tilde{a}_y(t,\tilde{x}) = a_y - (1/m)\hat{\theta} f_y^*(d, \hat{v}_x, \hat{v}_y, \hat{r})$. The functions η_{v_y} and η_θ remain the same as before; that is, they are functions of v_x and r, and not of the estimates $\hat{v}_x$ and $\hat{r}$.[3] The notation $\Lambda = \Lambda(d,\hat{x})$, $\hat{f}_y^* = f_y^*(d, \hat{v}_x, \hat{v}_y, \hat{r})$, $\hat{f}_r^* = f_r^*(d, \hat{v}_x, \hat{v}_y, \hat{r})$, $\xi = \xi(d,\hat{x})$, $\zeta = \zeta(d,\hat{x})$, and $\tilde{a}_y = \tilde{a}_y(t,\tilde{x})$ is used for the sake of brevity.

The following observer is proposed:

$$\dot{\hat{v}}_x = a_x + r\hat{v}_y + \sum_{i=1}^{4} K_i(t)\left(v_{x,i} - \hat{v}_x\right), \quad (14a)$$

$$\dot{\hat{v}}_y = a_y - r\hat{v}_x + K_{v_y}\Lambda\xi\left(m a_y - \hat{\theta}\hat{f}_y^*\right) + \frac{\Gamma_2}{\Gamma_1}\zeta\left(r - \hat{r}\right), \quad (14b)$$

$$\dot{\hat{r}} = \frac{1}{J}\hat{\theta}\hat{f}_r^* + K_r\left(r - \hat{r}\right), \quad (14c)$$

$$\dot{\hat{\theta}} = \Gamma_1 K_{v_y}\Lambda\hat{f}_y^*\left(m a_y - \hat{\theta}\hat{f}_y^*\right) + \Gamma_2\hat{f}_r^*\left(r - \hat{r}\right), \quad (14d)$$

where K_r, Γ_1, and Γ_2 are positive gains. The values $K_i(t)$ are continuously chosen, time-varying gains, and $v_{x,i}$ are longitudinal velocities calculated from the individual wheel angular velocities and the yaw rate. For the stability proofs, the weighted average $\sum_{i=1}^4 K_i(t)v_{x,i}/\sum_{i=1}^4 K_i(t)$ is assumed to be an exact measurement of v_x (see Imsland et al. (2006a) for a detailed discussion of the longitudinal velocity estimation).

Theorem 3 (UGAS of full observer) *Suppose that Assumptions 1, 2′, and 3′ and the condition expressed by* (9) *hold. Then there exist constants $C_1 > 0$ and $C_2 > 0$ such that if the gains are chosen according to $\sum_{i=1}^4 K_i(t) > C_1$ and $K_r > C_2$, then the origin of the error dynamics corresponding to the observer* (14) *is* UGAS. □

[3] Note that (8) does not hold with the new definition of $\tilde{a}_y$.

PROOF (OUTLINE) We define the LFC

$$V(\tilde{x}) = \frac{1}{2}(\Gamma_1\theta\tilde{v}_x^2 + \Gamma_1\theta\tilde{v}_y^2 + \Gamma_2 J\tilde{r}^2 + \tilde{\theta}^2).$$

Using the assumptions, it can be shown that with the proper selection of gains,

$$\dot{V}(t,\tilde{x}) \leq -c\left(\tilde{v}_x^2 + \tilde{r}^2 + \tilde{a}_y^2\right),$$

where c is some positive constant. We define $\phi(t,\tilde{x}) = a_y - (1/m)\hat{\theta} f_y^*(d, v_x, \hat{v}_y, r)$. It can be shown that for $(t,\tilde{x}) \in \mathbb{R} \times \overline{B}(\Delta)$, there exists a $K(\Delta)$ such that defining $Y\colon \mathbb{R}^4 \times \mathbb{R} \to \mathbb{R}$ as

$$Y(z,\psi) = -c(\|z_{\{1,3\}}\|^2 + \max\{\psi^2 - K(\Delta)|\psi|\|z_{\{1,3\}}\|, 0\})$$

yields $\dot{V}(t,\tilde{x}) \leq Y(\tilde{x}, \phi(t,\tilde{x}))$, $Y(z,\psi) \leq 0$, and $Y(z,\psi) = 0 \implies z_{\{1,3\}} = 0$, $\psi = 0$. The rest of the proof follows along the same lines as the proof of Theorem 1 with the Uδ-PE condition imposed on the function ϕ instead of $\tilde{a}_y$. ■

Theorem 4 (ULES of full observer) *Suppose that Assumptions 1, 2′, and 3′ and the condition expressed by* (9) *hold. Then there exist constants $C_1 > 0$ and $C_2 > 0$ such that if the gains are chosen according to $\sum_{i=1}^{4} K_i(t) > C_1$ and $K_r > C_2$, then the origin of the error dynamics corresponding to the observer* (14) *is* ULES. □

PROOF (OUTLINE) The proof follows along the same lines as the proof of Theorem 2, using the LFC

$$V_{\mathrm{PE}}(t,\tilde{x}) = V(\tilde{x}) - \gamma \int_t^\infty \mathrm{e}^{t-\tau}\phi^2(\tau,\tilde{x})\,\mathrm{d}\tau,$$

where V and ϕ are defined in the proof of Theorem 3. ■

Remark 4 The constants C_1 and C_2 in Theorems 3 and 4 depend on K_{v_y}, Γ_1, and Γ_2, which must be chosen first. □

6 Approximation of ξ and ζ

In Assumption 3′, it is assumed that we can obtain values $\xi(d,\hat{x})$ such that (12) holds exactly. The challenge is to find the gradient of the line connecting the values $f_y^*(d,\hat{v}_x,v_y,\hat{r})$ and $f_y^*(d,\hat{v}_x,\hat{v}_y,\hat{r})$. In general, the exact values cannot be found, because v_y is unavailable, but the shape of this function makes the task of approximating the value appealing. In Imsland et al. (2006a, Assumption 2), it is assumed that the friction model fulfills the condition $[\partial f_y^*/\partial v_y](d,v_x,v_y,r) \leq c < 0$ within a region. For the purpose of estimating ξ, we instead make the assumption that for all $(d,v_x,v_y,r) \in D_d \times \mathbb{R}\times\mathbb{R}\times\mathbb{R}$, $[\partial f_y^*/\partial v_y](d,v_y,v_x,r) \leq 0$. According to this, ξ is always non-positive, and hence one possible approximation is a negative constant. Although extremely crude, this approximation is surprisingly effective. It is also a safe choice in the sense that it limits errors by ensuring that the feedback from $\tilde{a}_y$ in the lateral velocity estimation never disappears. A somewhat better solution is to use a truncated Taylor series expansion around some nominal value v_y^* or around the estimate $\hat{v}_y$. In the latter case, the ULES property of the origin of the error dynamics is guaranteed to be preserved (even without the above assumption). One may also use considerations of convexity and concavity to identify situations in which any error from the Taylor series expansion actually improves stability (see Annaswamy, Skantze, and Loh, 1998), and use this information to create an estimation scheme based on a combination of the above approaches. Experimental results indicate that errors in the approximation have little effect on performance as long as it is ensured that ξ is not close to zero for long periods of time. This is largely because any error in the approximation becomes a potential problem only if there is variation in the lateral velocity, which also when the robustness of the observer is greatest.

For approximating ζ, a Taylor series expansion around $\hat{v}_y$ is a good enough approximation, because the gain K_r can be used to suppress the error. Moreover, the actual values of ζ are small, so the term where this value enters in (14b), although necessary for the technical proofs, has a negligible impact on the estimates when the observer is properly tuned.

7 Excitation Condition

The excitation condition given by (9) is essential for the stability results presented in this paper, and despite its technical nature, it has an intuitively appealing interpretation. As explained in Remark 2, it concerns the relationship between two signals, $\eta_{v_y}(\cdot,\tilde{v}_y)$ and $\eta_\theta(\cdot,\tilde{v}_y)$. If $\tilde{v}_y$ is fixed at a specific value, then, essentially, the remaining time-varying signals affecting η_{v_y} and η_θ should cause $\eta_{v_y}(t,\tilde{v}_y)$ and $\eta_\theta(t,\tilde{v}_y)$ to vary independently within any time period of a certain length.

The functions η_{v_y} and η_θ depend nonlinearly on many different time-varying signals, which cause them to behave differently. In particular, the inequality $[\partial f_y^*/\partial v_y](d,v_x,v_y,r) \leq 0$ implies that $\eta_{v_y}(t,\tilde{v}_y)$ is non-positive at all times. By contrast, $\eta_\theta(t,\tilde{v}_y)$ varies much in the same way as the lateral acceleration, and is likely to frequently switch signs, at least for moderate values of $\tilde{v}_y$. Furthermore, we note that η_{v_y} and η_θ are essentially measures of the influence of $\tilde{v}_y$ and $\tilde{\theta}$ on $\tilde{a}_y$. The plots in Section 3.1 clearly indicate that the relation between these varies along the slip curves.

This translates into a requirement that the driving pattern should be somewhat varied; in particular, the condition will be satisfied if there is variation in the lateral velocity and acceleration. A certain amount of steering, acceleration, or braking in order to cause variation in the lateral tire slips is required. It is not necessary that this happen all the time, but by choosing a large enough T, it must be possible to guarantee some variation within any time interval of that length.

The intuitive appeal of this condition is clear: it is impossible to tell anything about the road surface conditions based

on the lateral movement of the vehicle, unless there is actually some variation in that movement. With this condition is mind, it is natural to distinguish between three general driving patterns.

7.1 Varied Lateral Velocity

If there is variation in the lateral velocity, the excitation condition will be fulfilled, and hence Theorems 3 and 4 apply. We may therefore expect convergence of all estimates.

7.2 Straight-Path Driving

If the vehicle is driven along a straight path for an indefinitely long time, the excitation condition will not be fulfilled. We state a separate result for this case.

Theorem 5 (Convergence during straight-path driving) *Suppose that Assumptions 1, 2′, and 3′ hold and that for each* $\varepsilon_1 > 0$*, there exists an* $\varepsilon_2 > 0$ *such that* $|\hat{v}_y| > \varepsilon_1$*,* $r = 0$*,* $\delta = 0 \implies |f_y^*(d, v_x, \hat{v}_y, 0)| > \varepsilon_2$*. If for all* $t \geq t_0$*,* $a_y = 0$*,* $v_y = 0$*,* $r = 0$*,* $\delta = 0$*, and* $\hat{\theta} \geq \theta_{\min} - \theta_\varepsilon > 0$*, then* $\lim_{t\to\infty}(\tilde{v}_x, \tilde{v}_y, \tilde{r}) = 0$*.* □

PROOF (OUTLINE) Using the Lyapunov function V from Theorem 3, Barbălat's lemma (Barbălat, 1959) can be used to conclude that $\lim_{t\to\infty}(\tilde{v}_x, \tilde{r}, \tilde{a}_y) = 0$. Using the extra condition in Theorem 5 and the continuity properties of f_y^*, it can be shown that this implies $\lim_{t\to\infty} \hat{v}_y = 0$. ■

Remark 5 In practical terms, the extra condition in Theorem 5 means that if the steering wheel angle is zero and the vehicle is not rotating, any nonzero lateral velocity will generate a nonzero lateral acceleration. This is reasonable from a physical point of view and is likely to hold for most friction models. The condition that $\hat{\theta} \geq \theta_{\min} - \theta_\varepsilon$ is ensured by parameter projection, as discussed in Section 3.2. □

7.3 Sustained Circle Maneuver

In a practical implementation, the estimates may begin to drift during particularly long-lasting circle maneuvers with little excitation. This type of situation can be detected, and a proper response can be built in. When the goal is estimation of vehicle side-slip, using an estimated friction parameter that is too high is far safer than using one that is too low, as explained by Fukada (1999). The response is therefore to let $\hat{\theta}$ be drawn toward a high value.

8 Experimental Validation

In this section, some results from practical testing of the observer in one passenger car with rear-wheel drive (Vehicle A) and one larger vehicle with four wheel drive (Vehicle B), are presented. For a detailed comparison between an EKF and an observer implementation similar to the one presented in this paper, see Imsland et al. (2007).

8.1 Practical Implementation

A discrete version of the observer is implemented using the forward Euler integration method with step size 0.01 s. The gains $K_i(t)$ for estimation of the longitudinal velocity are updated at each time step. [4] The measurements of longitudinal and lateral acceleration, yaw rate, steering wheel angle, and wheel angular velocities are provided by production-type sensors; and, for the purpose of observer validation, the longitudinal and lateral velocities are measured using optical correlation sensors. The nominal value of μ_H is set to $\mu_H^* = 1.0$, and the friction parameter bounds are chosen as $\theta_{\min} = 0.1$ and $\theta_{\max} = 1.0$.

8.1.1 Friction Model

The friction model used is a proprietary one of similar complexity to the Magic Formula, and it has not been modified for use in the observer. It has the desirable property that the slip curves, plotted in Figure 2, flatten out rather than descend for large slip values. This helps to ensure that the inequality $[\partial f_y^*/\partial v_y](d, v_x, v_y, r) \leq 0$ from Section 6 always holds for the model. This is desirable even if this inequality can be broken in the real system for brief periods of time, resulting in a limited model error. With the exception of wheel radius, the friction model is tuned with identical tire parameters for both vehicles, even though the actual tires used are different. The accelerations a_x and a_y are used in order to estimate the load distribution, and thereby the vertical normal force F_z for each wheel.

A relatively simple method based loosely on the discussion in Section 6 is chosen for approximation of ξ. Most of the time, $\xi = [\partial \hat{f}_y^*/\partial \hat{v}_y]$ and the scaling Λ is set to $1/\|[\xi, \hat{f}_y^*]\|$. But in certain cases, if $|ma_y| < |\hat{\theta}\hat{f}_y^*|$ and $[\partial \hat{f}_y^*/\partial \hat{v}_y] > -|\hat{f}_y^*|$, then $\xi = -|\hat{f}_y^*|$ and $\Lambda = 1/(2|\hat{f}_y^*|)$. The reason for not using the partial derivative at all times is a practical one, to ensure that enough weight is given to the feedback in the lateral velocity part of the observer (compared to the friction adaptation part), in situations where this has proven to be important through experimental results. The scaling Λ is saturated at $\Lambda_{\min} = 10^{-6}$ and $\Lambda_{\max} = 10^6$.

8.1.2 Monitoring of Excitation Condition

As discussed in Section 7.3, it is sensible to let the friction parameter be drawn toward a high value whenever there is insufficient excitation for estimation of the friction parameter. To approximately monitor the excitation condition, we look at variation in the value $\hat{f}_y^*/\|[\xi, \hat{f}_y^*]\|$. The value is high-pass filtered, squared, and then low-pass filtered. If the output is below a threshold value, the friction coefficient is drawn exponentially toward the value 1.

[4] For a description of how these are chosen, see Imsland, Johansen, Fossen, Kalkkuhl, and Suissa (2006b).

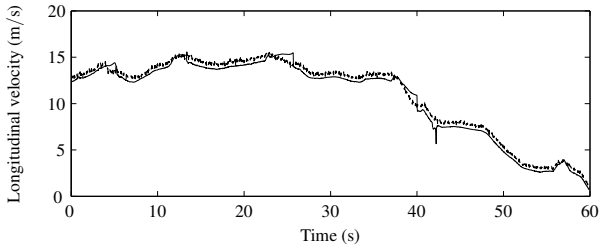

(a) Real (dashed) and estimated (solid) longitudinal velocity

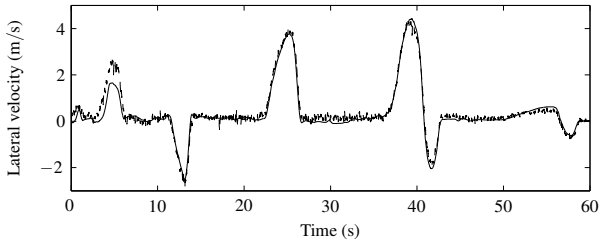

(b) Real (dashed) and estimated (solid) lateral velocity

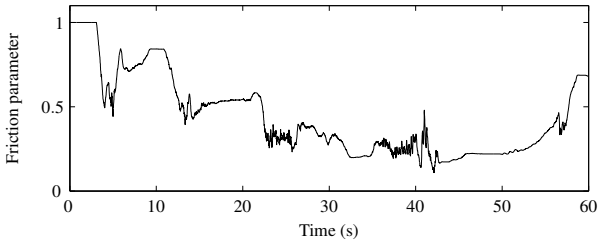

(c) Estimated friction parameter

Fig. 4. Results for Vehicle A on ice

8.1.3 Signal Processing in Update Law

Slow drift and bias in the lateral acceleration measurement influence the value $\tilde{a}_y$ in the observer error dynamics and has an adverse effect on performance. Because it is the dynamic behavior of $\tilde{a}_y$ that is useful for adaptation of the friction parameter, $\tilde{a}_y$ is high-pass filtered in the parameter update law, using the transfer function $s/(s+0.25)$.

8.2 Experimental Results, Vehicle A

The observer for Vehicle A is implemented using the gains $K_{v_y} = 1/m$, $K_r = 40$, $\Gamma_1 = 4$, and $\Gamma_2 = 0.1/J$. Results from the first test with Vehicle A are shown in Figure 4. The vehicle is driven on ice, mostly along a straight path with a few sharp turns. The adapted friction parameter varies largely in stages, changing quickly during turns and little between turns.

The second test represents a circle maneuver on asphalt, and the results can be seen in Figure 5. Throughout the first half of the test, the modification for handling low excitation is active, and hence the friction parameter remains constant. It then starts varying, but remains high.

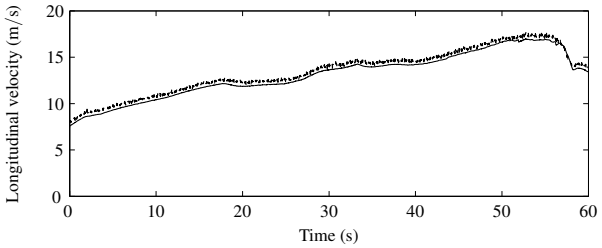

(a) Real (dashed) and estimated (solid) longitudinal velocity

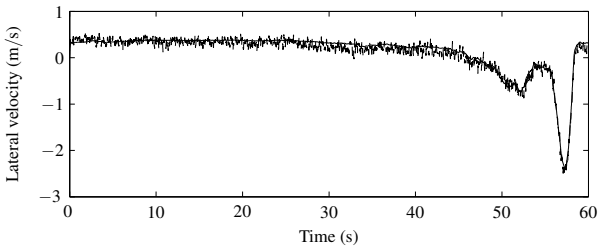

(b) Real (dashed) and estimated (solid) lateral velocity

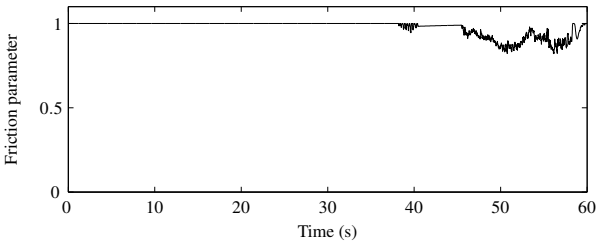

(c) Estimated friction parameter

Fig. 5. Results for Vehicle A on asphalt

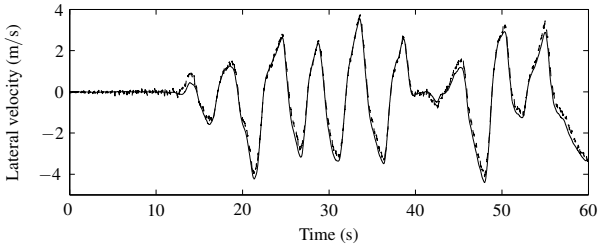

(a) Real (dashed) and estimated lateral velocity

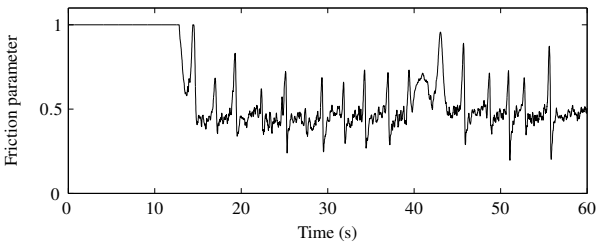

(b) Estimated friction parameter

Fig. 6. Results for Vehicle B on snow

8.3 Experimental Results, Vehicle B

The four-wheel drive complicates estimation of the longitudinal velocity for Vehicle B. For simplicity, the longitu-

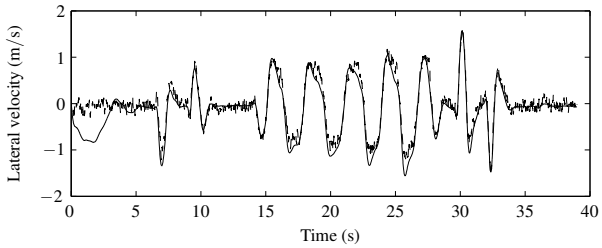

(a) Real (dashed) and estimated lateral velocity

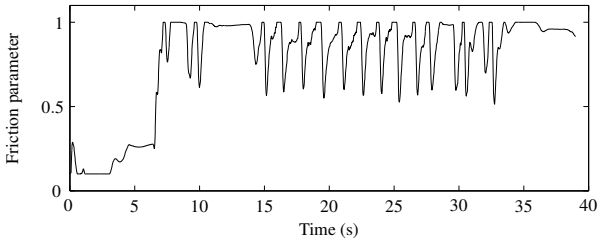

(b) Estimated friction parameter

Fig. 7. Results for Vehicle B on asphalt

dinal velocity measurement provided by the optical correlation sensor is therefore used in the tests presented here. The observer for Vehicle B is implemented with the gains $K_{v_y} = 1/m$, $K_r = 40$, $\Gamma_1 = 5$, and $\Gamma_2 = 1/J$. The first test is a slalom-like maneuver on a snow surface, with the results shown in Figure 6. For about 20 s, the vehicle is accelerated from about 1 m/s to approximately 21 m/s. Throughout the rest of the test, it mostly decelerates, to about 12 m/s at the end of the test. For the first part of the test, the low-excitation modification is active, but when the vehicle starts turning, the friction parameter starts quickly changing.

The final test is a slalom-like maneuver on asphalt, with the results shown in Figure 7. The longitudinal velocity varies relatively slowly in the range 21–30 m/s during the test. For this test, the initial value of the friction parameter is set much too low, at 0.1, which causes an initial inaccuracy.

The estimated friction parameter varies much more for Vehicle B than for Vehicle A. This indicates that the parameters used in the friction model are a better match for the tires on Vehicle A. The results for Vehicle B also indicate robustness with respect to errors in the friction model.

9 Concluding Remarks

In this paper, the results from Imsland et al. (2006a) are extended to create a nonlinear vehicle velocity observer with adaptation to different road surface conditions, and the stability properties of this observer are analyzed. Experimental results confirm that the method has merit and can function in real, non-ideal circumstances. The results also support the excitation condition found in the theoretical analysis and the practical interpretation of it.

The model used in this paper does not include the effect of any nonzero road bank angle, which will induce additional lateral forces on the vehicle and therefore have an adverse effect on estimation. In a final implementation, this should preferably be addressed through additional estimation of the road bank angle. Some discussion on this topic and on how it may be handled can be found in Imsland et al. (2007).

Acknowledgements

The authors wish to thank Dr. Antonio Loría for helpful discussion.

References

Annaswamy, A. M., Skantze, F. P., Loh, A.-P., 1998. Adaptive control of continuous time systems with convex/concave parametrization. Automatica 34 (1), 33–49.

Barbălat, I., 1959. Systèmes d'équations différentielles d'oscillations non linéaires. Rev. Math. Pures Appl. 4 (2), 267–270.

Best, M. C., Gordon, T. J., Dixon, P. J., 2000. An extended adaptive Kalman filter for real-time state estimation of vehicle handling dynamics. Vehicle System Dynamics 34, 57–75.

Canudas-de-Wit, C., Petersen, M. L., Shiriaev, A., 2003. A new nonlinear observer for tire/road distributed contact friction. In: Proc. 42nd IEEE Conf. Dec. Contr. Maui, HI.

Fukada, Y., 1999. Slip-angle estimation for vehicle stability control. Vehicle System Dynamics 32, 375–388.

Grip, H. F., Imsland, L., Johansen, T. A., Fossen, T. I., Kalkkuhl, J. C., Suissa, A., 2006. Nonlinear vehicle velocity observer with road-tire friction adaptation. In: Proc. 45th IEEE Conf. Dec. Contr. San Diego, CA.

Gustafsson, F., 1997. Slip-based tire-road friction estimation. Automatica 33 (6), 1087–1099.

Hac, A., Simpson, M. D., 2000. Estimation of vehicle side slip angle and yaw rate. In: Proc. SAE World Congress. Detroit, MI.

Imsland, L., Grip, H. F., Johansen, T. A., Fossen, T. I., Kalkkuhl, J. C., Suissa, A., 2007. Nonlinear observer for vehicle velocity with friction and road bank angle adaptation – validation and comparison with an extended Kalman filter. In: Proc. SAE World Congress. Detroit, MI.

Imsland, L., Johansen, T. A., Fossen, T. I., Grip, H. F., Kalkkuhl, J. C., Suissa, A., 2006a. Vehicle velocity estimation using nonlinear observers. Automatica 42 (12), 2091–2103.

Imsland, L., Johansen, T. A., Fossen, T. I., Kalkkuhl, J. C., Suissa, A., 2006b. Nonlinear observer for vehicle velocity estimation. In: Proc. SAE World Congress. Detroit, MI.

Ioannou, P. A., Sun, J., 1996. Robust Adaptive Control. Prentice Hall, Upper Saddle River, NJ.

Khalil, H. K., 2002. Nonlinear Systems, 3rd Edition. Prentice Hall, Upper Saddle River, NJ.

Kiencke, U., Nielsen, L., 2000. Automotive Control Systems. Springer.

Loría, A., de León Morales, J., 2003. On persistently exciting observers and a non-linear separation principle: application to the stabilization of a generator. Int. J. Contr. 76 (6), 607–617.

Loría, A., Panteley, E., Popović, D., Teel, A. R., 2005. A nested Matrosov theorem and persistency of excitation for uniform convergence in stable nonautonomous systems. IEEE Trans. Automat. Contr. 50 (2), 183–198.

Loría, A., Panteley, E., Popović, D., Teel, A. R., 2006. Persistency of excitation for uniform convergence in nonlinear control systems. Univ. California, Davis, CA [Online], available: http://front.math.ucdavis.edu/math.OC/0301335.

Nishira, H., Kawabe, T., Shin, S., 1999. Road friction estimation using adaptive observer with periodical σ-modification. In: Proc. IEEE Int. Conf. Contr. Appl. Kohala Coast, HI.

Ono, E., Asano, K., Sugai, M., Ito, S., Yamamoto, M., Sawada, M., Yasui, Y., 2003. Estimation of automotive tire force characteristics using wheel velocity. Contr. Eng. Pract. 11, 1361–1370.

Ortega, R., Fradkov, A., 1993. Asymptotic stability of a class of adaptive systems. Int. J. Adapt. Contr. Signal Process. 7 (4), 255–260.

Pacejka, H. B., 2006. Tire and Vehicle Dynamics, 2nd Edition. Butterworth-Heinemann.

Panteley, E., Loría, A., Teel, A., 2001. Relaxed persistency of excitation for uniform asymptotic stability. IEEE Trans. Automat. Contr. 46 (12), 1874–1886.

Ray, L. R., 1997. Nonlinear tire force estimation and road friction identification: Simulation and experiments. Automatica 33 (10), 1819–1833.

Suissa, A., Zomotor, Z., Böttiger, F., 1994. Method for determining variables characterizing vehicle handling. US Patent 5,557,520, filed Jul. 29, 1994; issued Sep. 17, 1996.

Young, N., 1988. An introduction to Hilbert space. Cambridge University Press, Cambridge, United Kingdom.

Zhang, Y., Ioannou, P. A., Chien, C.-C., 1996. Parameter convergence of a new class of adaptive controllers. IEEE Trans. Automat. Contr. 41 (10), 1489–1493.

Åström, K.-J., Bohlin, T., 1965. Numerical identification of linear dynamic systems from normal operating records. In: Hammond, P. (Ed.), Proc. 2nd IFAC Symp. Theory of Self-adaptive Control Systems. Teddington, U.K.